10.89

Hydraulics Research
Wallingford

AN EFFICIENT COMPUTATIONAL MODEL
FOR WAVE REFRACTION AND DIFFRACTION
USING FINITE DIFFERENCES

H N Southgate MA
D G Goldberg BA

Report SR 213
June 1989

Registered Office: Hydraulics Research Limited,
Wallingford, Oxfordshire OX10 8BA.
Telephone: 0491 35381. Telex: 848552

This report describes work carried out by Hydraulics Research under Commission 14D1 funded by the Ministry of Agriculture, Fisheries and Food, nominated officer Mr A J Allison. At the time of reporting this project, Hydraulics Research's nominated project officer was Dr S W Huntington.

ABSTRACT

A new type of computational wave transformation model is described in this report. The model incorporates the processes of wave refraction and diffraction, and uses a time-independent finite-difference marching technique. The model is computationally more efficient than most alternative techniques which combine refraction and diffraction in a general manner. Tests are carried out on a circular shoal depth profile, a situation for which strong diffraction effects occur.

CONTENTS

1 INTRODUCTION

This report is concerned with a new type of computational wave transformation model incorporating the combined effects of refraction and diffraction of waves using a time-independent finite-difference marching technique. This method has several potential advantages over alternative techniques. The inclusion of diffraction should give improved predictions of wave parameters compared with pure refraction methods in areas of irregular bathymetry where diffraction effects are strong. The method is also computationally quicker than most alternative refraction-diffraction methods, with the possibility of further increasing computational speed by the ability to use coarser grid sizes. Random wave spectra, current refraction effects, and dissipation by bottom friction and breaking can be included, but the tests described in this report are concerned with the basic wave processes of depth refraction and diffraction for monochromatic waves. The model is designed for wave propagation in the open sea, rather than where structures are present. Wave directions are limited to a certain range either side of the forward grid direction, although the tests presented here indicate that the model can be used for wave directions at more than 40° from this forward grid direction.

The report is structured as follows. Chapter 2 contains the theory on which the model is based, and Chapter 3 describes the finite-difference scheme and numerical techniques. In Chapter 4 the model is applied to the problem of wave propagation over a circular shoal. Classical ray theory predicts a cusped caustic for this problem and therefore, in nature, strong diffraction effects are present. The circular shoal problem thus represents quite a severe test case for the model. Finally, the main conclusion from the study are summarised in Chapter 5.

2 THEORY

The model is based on a theoretical approach originally put forward by Battjes (1968). This approach, however, suffered from a lack of interest for many years, probably because it was felt that it had been superceded by the Mild-Slope Equation (Eq 1) which was formulated shortly afterwards (Berkhoff 1973 and 1976). Although models based on the Mild-Slope Equation have been successfully applied to long waves and relatively small enclosed sea areas, they have been found in many cases to be too computationally inefficient for short waves and large open-sea areas. In order to develop a model for these latter types of problem, Yoo and O'Connor (1986 and 1988) have returned to and extended Battjes' approach. The model described in this report uses the same theoretical basis as Yoo and O'Connor but adopts a different numerical modelling approach. Yoo and O'Connor used a time-dependent formulation which can require a considerable number of time steps to reach a steady state. The present model is time-independent and gives the steady state solution directly.

The governing equations used by the model can be derived from the time-independent form of the Mild-Slope Equation,

$$\nabla . \; (cc_g \; \nabla\eta) + \frac{\omega^2 \; c_g}{c} \, \eta = 0 \qquad (1)$$

in which η is the complex water surface elevation, c is the wave celerity, c_g is the wave group velocity, ω is the angular wave frequency, and ∇ is the two-dimensional horizontal gradient operator. η can in general be written as

$$\eta = Ae^{iS} \tag{2}$$

where A is the wave amplitude and S is the wave phase. Substituting Eq 2 into Eq 1 results in the following two equations:

$$(\nabla S)^2 = k^2 + \frac{\nabla^2 A}{A} + \frac{\nabla(cc_g)}{cc_g} \cdot \frac{\nabla A}{A} \tag{3}$$

$$\nabla . (A^2 \underline{c_g}) = 0 \tag{4}$$

k is the wave separation factor and is determined from known values of water depth (h) and angular wave frequency (ω) by the linear dispersion relation

$$\omega^2 = gk \tanh (kh) \tag{5}$$

c and c_g are given by the expressions,

$$c = \frac{\omega}{k} \tag{6}$$

$$c_g = \frac{c}{2}(1 + \frac{2kh}{\mathrm{Sinh}(2kh)}) \tag{7}$$

The last two terms on the right-hand side of Eq 3 represent diffraction effects. The omission of these terms gives the refraction approximation used in ray tracing models. Under this approximation k is equivalent to the wavenumber, $K = \underline{\nabla}S$. The present model retains the $\nabla^2 A/A$ term which is usually much larger than the final term in Eq 3. The system of equations solved by the model can therefore be written as

$$\nabla \times \underline{K} = \underline{0} \tag{8}$$

$$K^2 = k^2 + \frac{1}{H}\nabla^2 H \tag{9}$$

$$\nabla . (H^2 \underline{c_g}) = 0 \tag{10}$$

in which $\underline{K}(=\nabla S)$ is the wavenumber, $H(=2A)$ is the wave height, and underlines denote vector quantities. Eq 8 expresses the identity $\nabla \times (\nabla S) = \underline{0}$.

These equations can be represented in Cartesian coordinates x, y:

$$\frac{\partial P}{\partial y} = \frac{\partial Q}{\partial x} \tag{11}$$

$$P^2 + Q^2 = k^2 + \frac{1}{H}\left(\frac{\partial^2 H}{\partial x^2} + \frac{\partial^2 H}{\partial y^2}\right) \tag{12}$$

$$\frac{\partial}{\partial x}(H^2 MP) + \frac{\partial}{\partial y}(H^2 MQ) = 0 \tag{13}$$

in which P is the x-component of $\underline{K}$, Q is the y-component of $\underline{K}$ and M is given by

$$M = \frac{c_g}{K} \tag{14}$$

The wave direction α is defined in Figure 1.

It is usual that the wave height curvature in the main propagation direction (y direction) is much less than in the lateral direction (x direction), and therefore $\partial^2 H/\partial y^2$ is neglected in Eq 12, although this approximation becomes less valid for small values of α. Furthermore, in order to use Eq 12 as a prediction equation for Q, it is differentiated with respect to y. Performing this differentiation, and using Eq 11, gives

$$\frac{\partial Q}{\partial y} = \frac{1}{Q}\left(- P \frac{\partial Q}{\partial x} + k \frac{\partial k}{\partial y} + \frac{1}{2}\frac{\partial}{\partial y}\left(\frac{1}{H}\frac{\partial^2 H}{\partial x^2}\right)\right) \tag{15}$$

Eqs 11, 13 and 15 are the three equations to be solved in the model for the three unknowns P, Q and H.

3 FINITE-DIFFERENCE SCHEME

The sea area under study is represented by a grid composed of rectangular or square elements. The positive y direction is chosen to be in the main propagation direction of the waves (roughly perpendicular to the coastline). Most variables such as h, H, k, K and α are defined at the centre of each rectangular element, but P is defined at the centre of the left-hand boundary, and Q at the centre of the bottom boundary (see Fig 2). Rows (grid lines in the x-direction) are labelled by the subscript i, and columns (grid lines in the y-direction) by j. A dummy column of P values beyond the right-most column is required to maintain a laterally symmetrical system. It has been found that this staggered grid system gives the most accurate finite-difference representation of the governing equations.

The method of solution uses a row-by-row marching technique with a predictor and corrector calculation at each row. The input values of H, ω and α are specified at each grid element on the offshore row. The finite-difference representation of the governing equations is then used to make a calculation of these parameters on the second row. This is the predictor step. Using these values, a more accurate estimate of the y-derivatives can be made, and the calculation of parameters on row two is repeated with these 'corrected' y-derivatives. This corrector step can, in principle, be repeated an indefinite number of times, but in most cases one calculation is found to be sufficient. The whole predictor-corrector process is then repeated for row three, and the process continues until the last row, furthest inshore, is reached. The method employed is explicit throughout.

Q Prediction Equation

It is required to predict quantities on the jth row given known values along the j-1th row. The first quantity to be predicted is Q, using a finite difference form of Eq 15. The overall finite-difference scheme for this equation is

$$Q_{i,j} = \Delta y \; [k \frac{\partial k}{\partial y} - P \frac{\partial Q}{\partial x} + \frac{1}{2} \frac{\partial}{\partial y} (\frac{1}{H} \frac{\partial^2 H}{\partial x^2})]/Q_{i,j-1} + Q_{i,j-1} \tag{16}$$

The first term in the square brackets is known from differentiation of Eq 5. An average value of P in the second term is calculated by

$$P = (P_{i+1,j-1} + P_{i,j-1})/2 \text{ (predictor step)} \tag{17}$$

$$P = (P_{i,j} + P_{i+1,j} + P_{i,j-1} + P_{i+1,j-1})/4 \text{ (corrector step)} \tag{18}$$

$\partial Q/\partial x$ is determined by a weighted angle derivative method. A weighting factor, f, is defined according to

$$f = 0 \qquad \text{for } \alpha \le \alpha_1 \tag{19}$$

$$f = \frac{\alpha - \alpha_1}{\alpha_2 - \alpha_1} \qquad \text{for } \alpha_1 < \alpha < \alpha_2 \tag{20}$$

$$f = 1 \qquad \text{for } \alpha \ge \alpha_2 \tag{21}$$

in which α_1 and α_2 are the angles from the (i,j-1) grid point to the (i+1,j) and (i-1,j) grid points respectively (see Fig 1). The following formulae are then used for $\partial Q/\partial x$,

$$\frac{\partial Q}{\partial x} = [(1-f)(Q_{i,j-1} - Q_{i-1,j-1}) + f(Q_{i+1,j-1} - Q_{i,j-1})]/\Delta x$$

(predictor step) (22)

$$\frac{\partial Q}{\partial x} = [(1-f)(Q_{i,j-1} - Q_{i-1,j-1} + Q_{i+1,j} - Q_{i,j})$$

$$+ f(Q_{i+1,j-1} - Q_{i,j-1} + Q_{i,j} - Q_{i-1,j})]/(2\Delta x)$$

(corrector step) (23)

The third term in the square brackets in Eq 16 is represented according to:

$$\frac{\partial}{\partial y}\left(\frac{1}{H}\frac{\partial^2 H}{\partial x^2}\right) = [(H_{i+1,j-1} - 2H_{i,j-1} + H_{i-1,j-1})/H_{i,j-1}$$

$$- (H_{i+1,j-2} - 2H_{i,j-2} + H_{i-1,j-2})/H_{i,j-2}]/\Delta y(\Delta x)^2$$

(predictor step) (24)

$$\frac{\partial}{\partial y}\left(\frac{1}{H}\frac{\partial^2 H}{\partial x^2}\right) = [(H_{i+1,j} - 2H_{i,j} + H_{i-1,j})/H_{i,j}$$

$$- (H_{i+1,j-1} - 2H_{i,j-1} + H_{i-1,j-1})/H_{i,j-1}]/\Delta y(\Delta x)^2$$

(corrector step) (25)

<u>P Prediction Equation</u>

A finite difference representation of the irrotationality equation, Eq 11, is used.

$$P_{i,j} = (Q_{i,j} - Q_{i-1,j})\,\Delta y/\Delta x + P_{i,j-1} \qquad (26)$$

(predictor and corrector steps)

In this equation, the value of Q at the current row is used. Therefore the P calculation comes after the Q calculation.

H Prediction Equation

A weighted angle derivative representation of Eq 13 is used. A weighting factor f is defined in the same manner as for the Q prediction method (Eqs 19-21) and the following definitions are made,

$$p = H^2MP \tag{27}$$

$$q = H^2MQ \tag{28}$$

The overall finite-difference scheme for Eq 13 is

$$q_{i,j} = - p \frac{\Delta y}{\Delta x} + q_{i,j-1} \tag{29}$$

The value of p is calculated by

$$p = (1-f)(p_{i,j-1} - p_{i-1,j-1}) + f(p_{i+1,j-1} - p_{i,j-1})$$
(predictor step) (30)

$$p = [(1-f)(p_{i,j-1} - p_{i-1,j-1} + p_{i+1,j} - p_{i,j})$$

$$+ f(p_{i+1,j-1} - p_{i,j-1} + p_{i,j} - p_{i-1,j})]/2 \tag{31}$$
(corrector step)

Once $q_{i,j}$ has been determined from Eqs 29-31, the wave height is given by

$$H_{i,j} = \left(\frac{q_{i,j}}{M_{i,j}\, Q_{i,j}}\right)^{½} \tag{32}$$

Stability

The model has been run on a circular shoal bathymetry which provides quite a severe test case. It was found that the finite-difference scheme gave numerically unstable results, and as a consequence much of the work in developing the model has been devoted to devising modifications to ensure stability. The governing equations do not readily lend themselves to an analytical investigation of stability, and therefore a number of ad hoc approaches have been tried. The most successful of these has involved forming averages of various quantities with neighbouring values along each row, according to the formula,

$$b_{n,i} = (\lambda b_{o,i-1} + 2(2-\lambda)b_{o,i} + \lambda b_{o,i+1})/4 \tag{33}$$

in which b denotes any predicted wave variable, and the subscripts o and n denote old (before averaging) and new (after averaging) values respectively. λ is an input parameter, between 0 and 2, which denotes the 'strength' of the averaging process. The strength of averaging can be expressed by the value of N in the ratio,

$$\lambda : 2(2-\lambda) : \lambda = 1 : N : 1 \tag{34}$$

λ is given in terms of N by

$$\lambda = \frac{4}{N + 2} \tag{35}$$

The averaging process can be repeated a number of times.

The use of this averaging process introduces some numerical dispersion in the model which has the effect of decreasing maxima and increasing minima of wave height. The most accurate results are found to be obtained when just sufficient averaging is used to ensure stability.

4 RESULTS

The testing of the model has been carried out using a circular shoal depth profile. This is a classical test case in which the shoal acts as a lens, focussing the wave rays into a cusped caustic (see Fig 3). In the region of the cusp the ray method breaks down and strong diffraction effects occur. Other researchers have studied this problem to assess the performance of alternative refraction-diffraction models. These include Ito and Tanimoto (1973) who used a type of time-dependent Mild-Slope Equation, Radder (1979) who used a time-independent parabolic method, and Yoo and O'Connor (1986 and 1988) who used a time-dependent form of the equations in this report.

The dimensions of the grid and circular shoal are identical to those used by Radder (1979), being 20m and 30m in the x-direction and y-direction respectively, while the depth profile over the shoal was defined by:

$$h = h_m + \frac{(h_0 - h_m)r^2}{R^2} \qquad (36)$$

in which h = depth at a general point over the shoal,

r = the distance from this general point to the centre of the shoal,

h_0 = the constant depth of the rest of the grid area (in this case 0.9375m),

h_m = is the minimum depth at the centre of the shoal (0.3125m),

and R = the radius of the shoal (5m).

The shoal has a circular cross-section in a horizontal plane, and a parabolic cross-section in a vertical plane, and is centred at x=10m, y=10m (see Fig 4).

Throughout the tests, the same offshore wave height and period (2.5m, 1.265s) were used as input to the model, with only the incident wave direction, α, being varied. As described in Section 2, α is defined as the angle between the positive x-axis and the direction that the wave is travelling towards, so that normal incidence is given by $\alpha = 90°$ (see Fig 1). A large number of different incident angles were used, but in this report, results are presented only for α equalling 90°, 70° and 50°, these being representative of a wide range of all possible incident angles. Indeed, 50° was considered to be a very stringent test of the model's abilities, since in most physical situations, one would expect the peak energy direction to be close to the normal.

Initial tests with a square grid spacing displayed instabilities. In order to solve this problem, without using a prohibitively small grid spacing, the spacings in the y-direction were halved with respect to those in the x-direction. A variety of different spacings were then used, corresponding to an 8th, a 16th and a 32nd of a wavelength in the x-direction, and, of course, half this in the y-direction. These are referred to in this report as the 'coarse', 'medium' and 'fine' grids respectively.

Furthermore, the parameter λ, the so-called 'strength of averaging', was varied for each grid spacing. The values used were 1, ½ or ¼. Halving λ essentially halves the effective grid size, since it is the equivalent of averaging a value with the values of two 'pseudo'-points on either side, these being calculated by interpolation between the value of the original point and those at its neighbours. However, the lower the value of this parameter, the more the tendency for instability.

It was also possible to vary the number of averagings performed in order to ensure stability. Of course, the general effect of averaging will be to increase stability at the cost of accuracy, since averaging will tend to bring peaks down and troughs up towards a mean level. Thus a balance had to be struck between these two necessary goals. Unsurprisingly, the larger the grid size, the higher was the number of averagings required to maintain stability. In some extreme cases, it was not even possible to attain the required balance between stability and accuracy without reducing the grid size.

Finally, it was possible as well to vary the number of times the corrector step in the marching scheme was performed (see Section 3). However, after various different trials, it was found that while one corrector step was necessary to attain the required level of accuracy and stability, little was achieved by having more than one. Thus, all the results presented in this report are from runs where the number of corrector steps is one.

Previous works on the same shoal with similar input conditions (see Refs 4 and 8) indicate that, with an incident wave height of 1m, there should be a slight decrease in wave height around the shoal, and then a steady increase, slowly at first and then more rapidly passing up the shoal, to about 1.3m over the centre, and reaching a maximum of about 2m over the opposite end of the shoal. Beyond the shoal, the wave height decreases gradually with smaller, subsidiary maxima and minima forming on either side. There is a line of symmetry through the centre of the shoal at the angle of incident wave direction.

The range of amplitudes obtained from various runs of the model is shown in Table 1. However, the clearest way of seeing the output from the model in detail is in the form of a wave amplitude contour plot. A variety of these is shown in Figures 5-10. Also, three isometric plots of wave amplitude are shown in Figures 11-13. These clearly show the shape of the output as described in the above paragraph. As can be seen, qualitatively, the results are exactly as expected. However, to attain high accuracy requires slightly more subtlety. For each set of input conditions, it was found that the best results were obtained when just enough averaging was used, with the highest possible value of λ, to ensure stability. In practice, this meant halving λ every time the grid size doubled and sometimes using more averaging. For example, Figure 5 shows the wave amplitude contour plot for normal incidence with λ equal to 1.0 in the fine grid. One averaging was used. Figure 6 shows the plot for the same offshore conditions run over the medium grid with λ halved to 0.5. The plots are almost identical. However, the similar run on the coarse grid with λ again reduced turned out to be unstable with only one averaging.

The effect of increasing the number of averagings can be seen by examining Figures 7 and 8. These are both output from runs over the fine grid with λ equal to 1.0 and an incident angle of 70°. However, the run shown in Figure 1 has only one averaging, while that shown in Figure 2 has 2. In the former figure, the contours are, in general, closer together indicating a rapid change in wave amplitude, the maximum is higher and the minimum lower, while in the latter, the changes in amplitude are slower and smoother.

It was also found that the larger the grid size, and the greater the deviation of incident wave direction from normal incidence, the greater the tendency for instability and thus, the more averaging that had to be performed in such cases to maintain stability. This trend can be seen clearly by looking at the positions of blocks of runs where instabilities were evident in Table 1. For example, Figure 9 shows the wave amplitude contour plot for the run over the fine grid with λ equal to one, a 50° incident wave and two averagings. As can clearly be seen, some instability is evident on the down-slope of the shoal. Figure 10 shows the contour plot for the same run but with three averagings. In this run, stability has just been restored, but without loss of accuracy - the plot looks like Figure 5 turned through 40°.

Ideally, it would have been desirable to derive, hueristically at least, some relationship between the input conditions, the depth grid and the averaging parameters in order to dictate necessary conditions for stability. However, with such a large number of variables, it was not possible, in practice, to derive such a relationship, or even to ascertain if one did actually exist. But this is not a serious limitation since, with the model running as rapidly as it does, finding the correct averaging parameters by trial and error is not a big problem. Furthermore, the user quickly acquires a feel for how the model will perform after a very few test runs.

5 CONCLUSIONS

In this report, we have presented, with results, a new type of computational wave transformation model which incorporates the combined effects of refraction, diffraction and shoaling of waves using a time-independent, finite-difference marching technique. The advantages of this model over previous finite-difference models are increased computational speed and the possibility of employing a coarser grid, thus cutting down the required computer space and time, while still maintaining a high degree of accuracy. Furthermore, the model has several advantages over traditional ray-tracing models too, since these necessarily ignore diffraction effects. The price to pay for these improvements has been the necessity to introduce two averaging parameters which must be chosen carefully, depending on depth, input conditions and grid size, in order to achieve both stability and accuracy. However, since the model runs in such a short time, it is usually a simple matter to obtain satisfactory values for these parameters by trail and error without too much effort. It is to be hoped that, after further use of the model in real situations, a more definite method of optimising the averaging parameters may be found. Despite this, the model has been found to be both accurate and efficient and should be of value in determining wave conditions at places where shoaling, refraction and diffraction of waves is significant.

6 REFERENCES

1. BATTJES J A. "Refraction of water waves", Journal of Waterway and Harbour Division, ASCE, Vol 94, WW4, pp 437-451, 1968.

2. BERKHOFF J C W. "Computation of combined refraction and diffraction", Proc. 13th Int. Conf. on Coastal Eng., Vancouver, ASCE, Vol 1, pp 471-490, 1973.

3. BERKHOFF J C W. "Mathematical models of simple harmonic linear water waves. Wave diffraction and refraction", Pub. no. 163, Delft Hydraulics Laboratory, Holland, 1976.

4. ITO Y and TANIMOTO K. "A method of numerical analysis of wave propagation. Application to wave diffraction and refraction", Proc. 13th Int. Conf. on Coastal Eng., Vancouver, ASCE, Vol 1, pp 503-522, 1973.

5. RADDER A C. "On the parabolic equation method for water-wave propagation, Journal of Fluid Mechanics, Vol 95, Part 1, pp 159-176, 1979.

6. SOUTHGATE H N. "The parabolic method for numerical modelling of water waves", Hydraulics Research, Report no. SR 81, March 1986.

7. YOO D and O'CONNOR B A. "Ray model for caustic gravity waves", Proc. 5th Conf. of Asian and Pacific Division of IAHR, Seoul, Vol 3, pp 1-13, 1986.

8. YOO D and O'CONNOR B A. "Diffraction of waves in caustics", Journal of Waterway, Port, Coastal and Ocean Division, ASCE, Vol. 114, No. 6, 1988.

TABLE

TABLE 1 Range of wave amplitudes for various runs

Angle of incidence		Number of Averagings 1	2	3
	F	0.69-1.76	0.82-1.47	0.87-1.32
50°	M	0.70-1.75	0.82-1.45	0.87-1.31
	C	0.87-1.21	0.82-1.43	0.87-1.29
	F	0.38-1.91	0.59-1.69	0.70-1.52
70°	M	0.13-1.92*	0.59-1.68	0.72-1.50
	C	0.05-1.95*	0.56-1.66	0.73-1.48
	F	*	0.55-1.92	0.63-1.92
50°	M	0.48-1.98*	0.56-2.06*	0.34-1.95
	C	0.30-2.18*	0.26-2.05*	0.25-1.92

NOTE: F = Fine grid, ($\lambda = 1$)
M = Medium grid, ($\lambda = \frac{1}{2}$)
C = Coarse grid, ($\lambda = \frac{1}{4}$)

The figures shown are minimum-maximum wave amplitudes in metres.

* indicates instability

FIGURES.

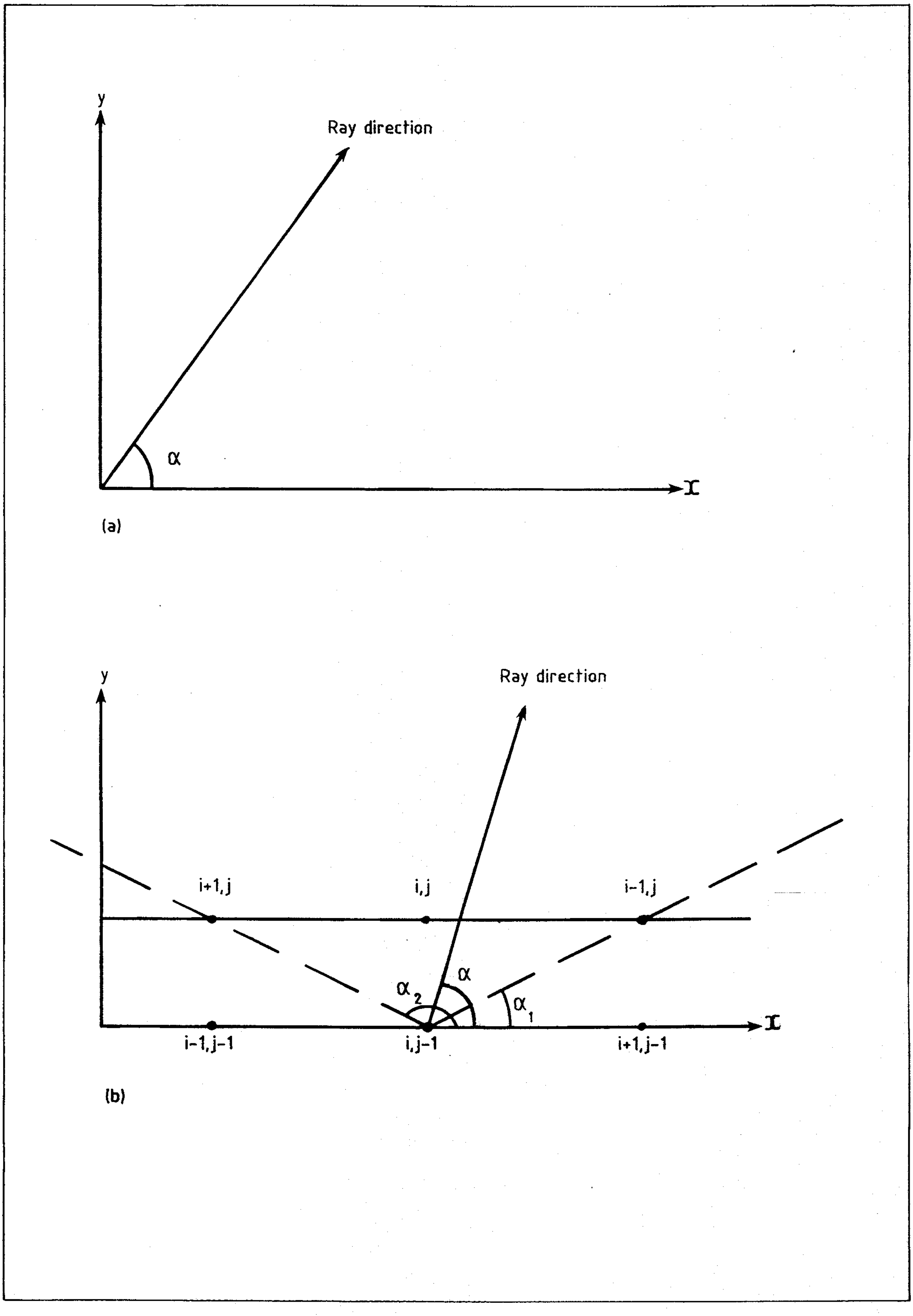

Fig 1 (a) Definition of wave ray direction α
(b) Definition of limiting angles α_1 and α_2 used in eqs. 19–21

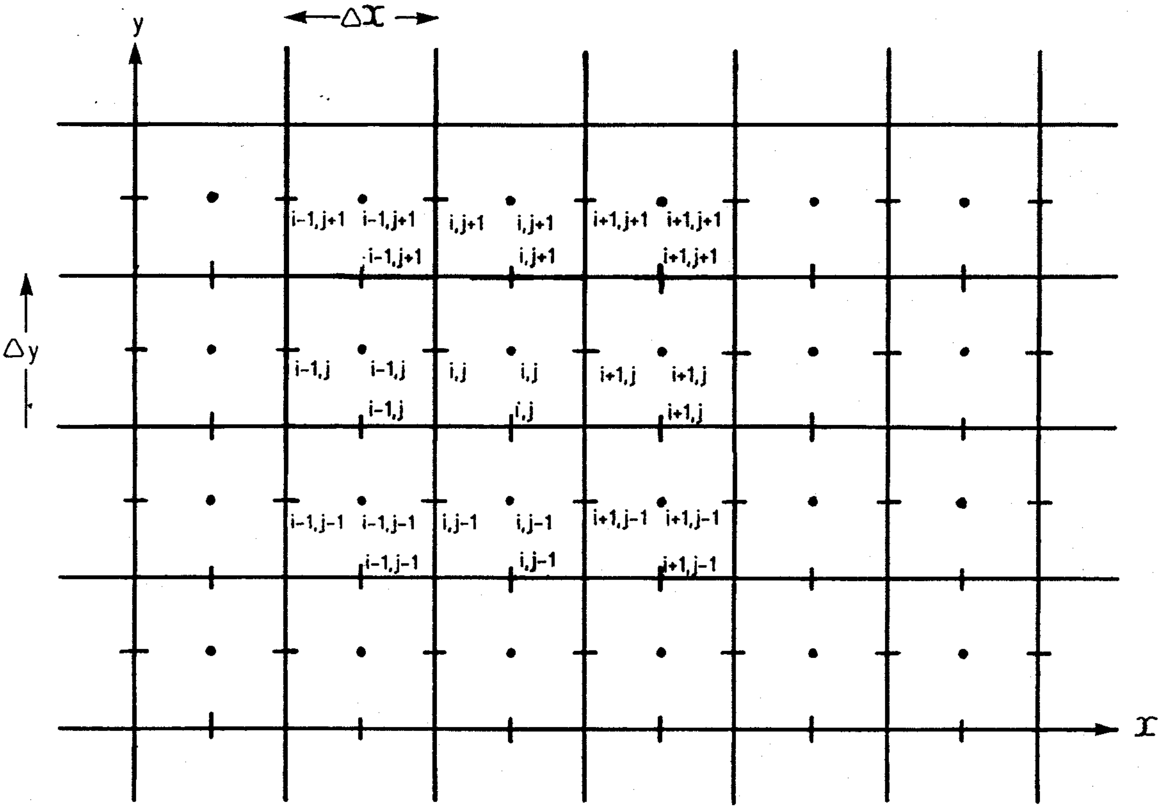

• $h, H, \mathcal{K}, k, \alpha$ defined at these points

— $P \equiv \mathcal{K} \cos \alpha$ defined at these points

| $Q \equiv \mathcal{K} \sin \alpha$ defined at these points

Fig 2 Grid system for the finite - difference scheme

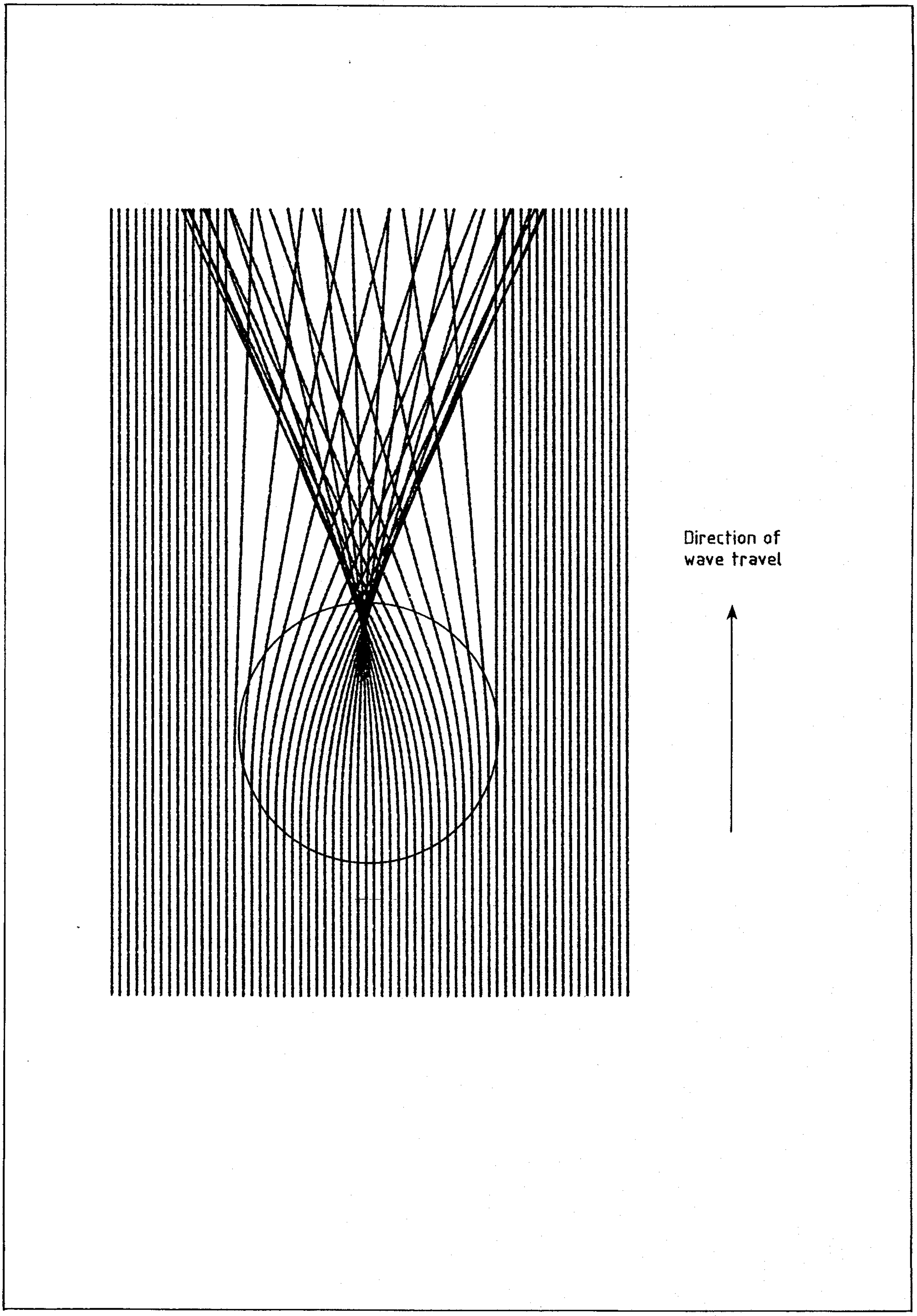

Fig 3 Ray diagram for waves travelling over circular shoal, showing formation of cusped caustic

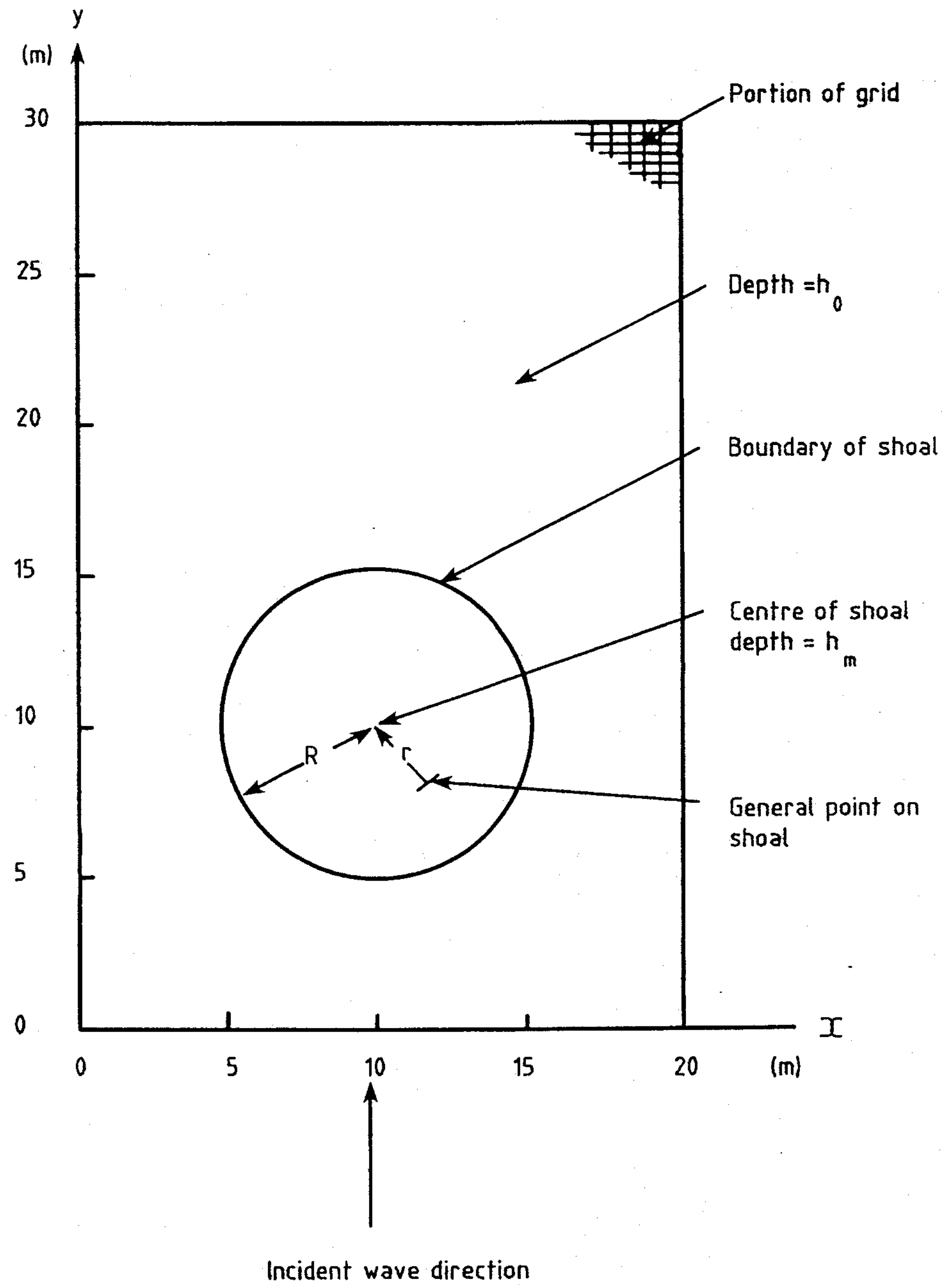

Fig 4 Model layout and grid for the circular shoal problem

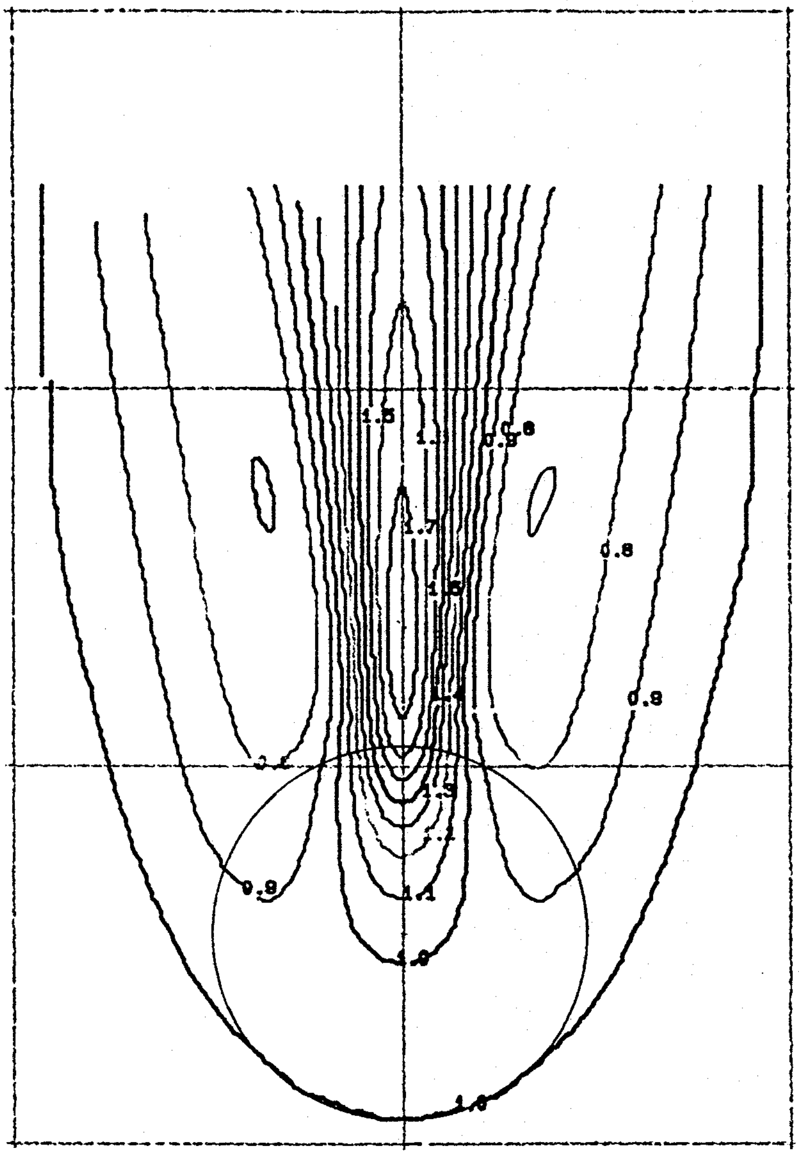

Fig 5 Wave amplitude contours, 90° incident direction, fine grid, averaging number=1

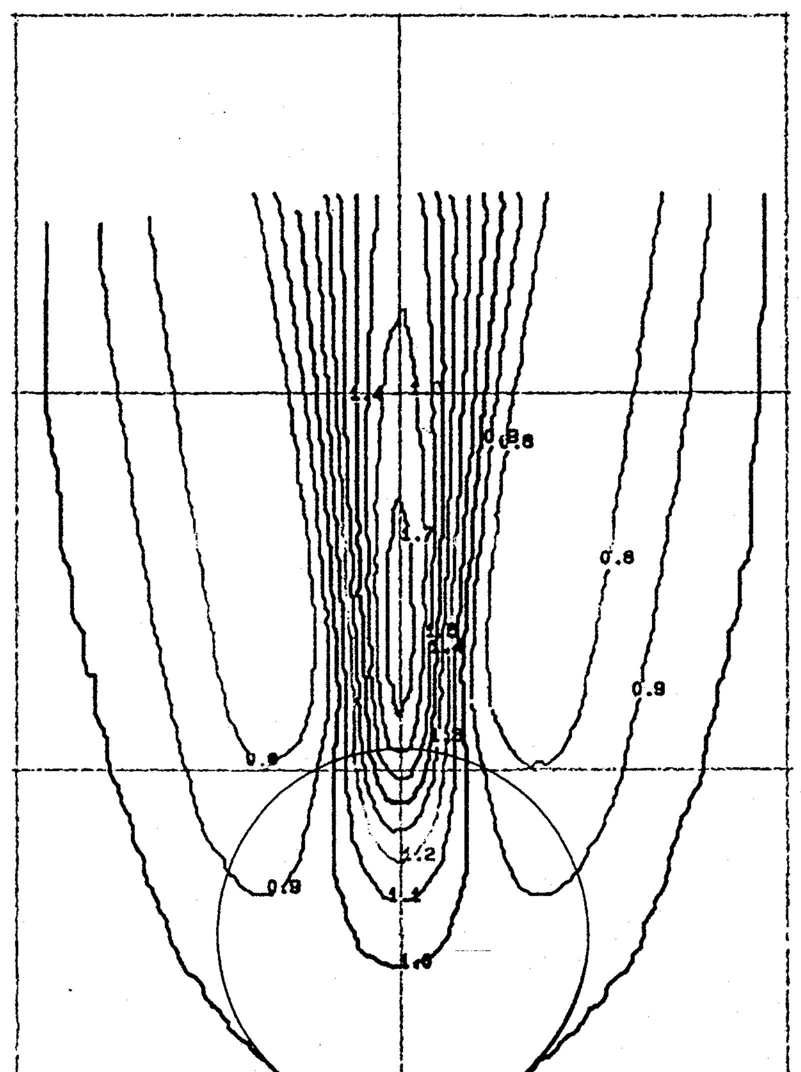

Fig 6 Wave amplitude contours, 90° incident direction, medium grid, averaging number=1

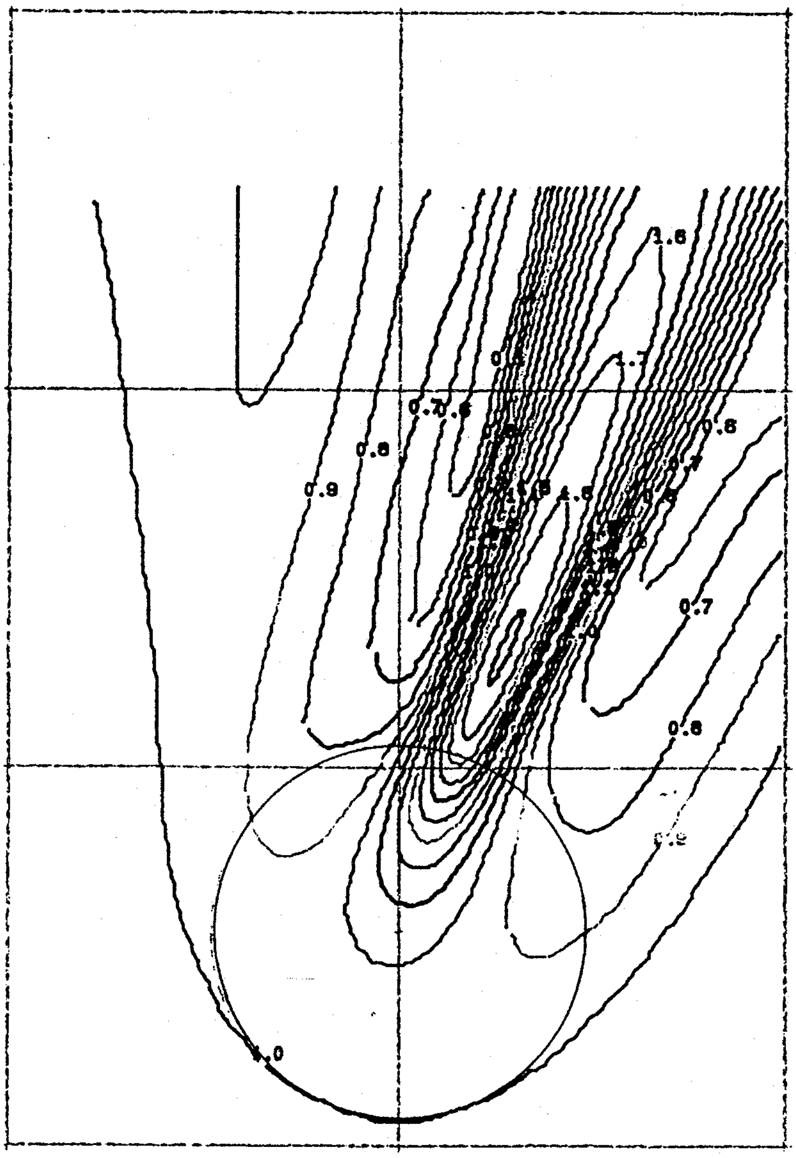

Fig 7 Wave amplitude contours, 70° incident direction, fine grid, averaging number=1

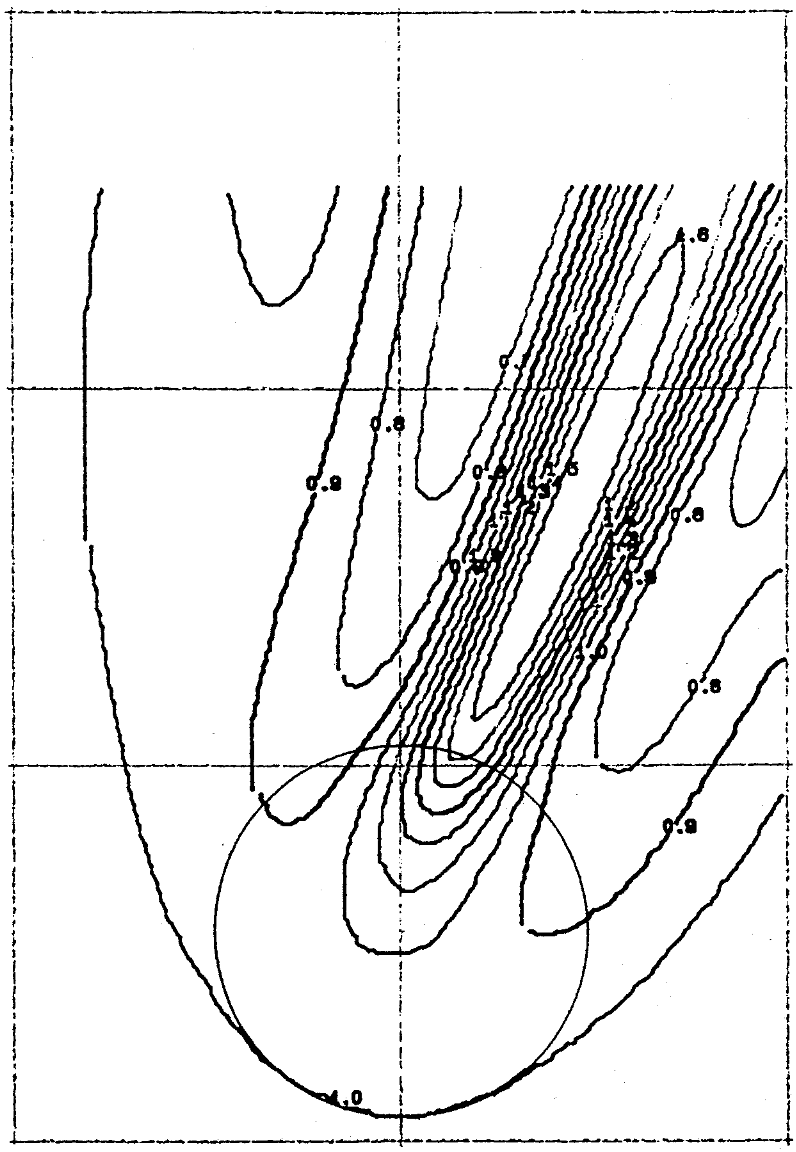

Fig 8 Wave amplitude contours, 70° incident direction, fine grid, averaging number=2

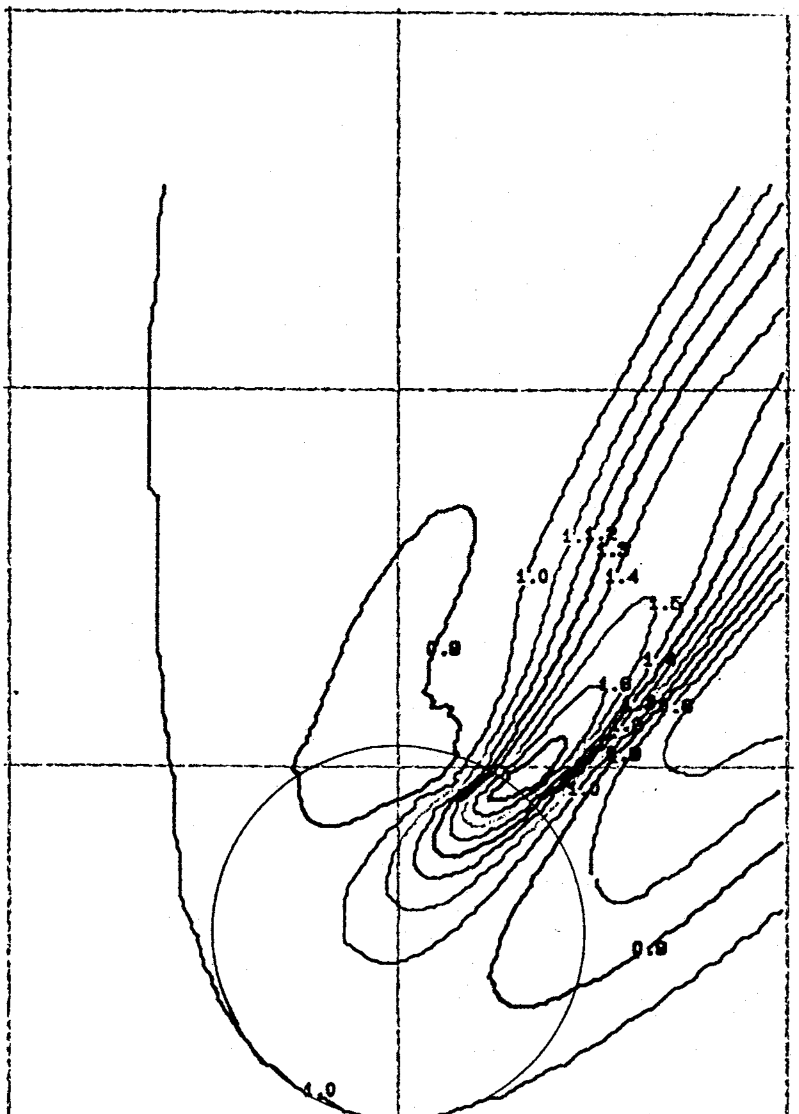

Fig 9 Wave amplitude contours, 50° incident direction, fine grid, averaging number=2

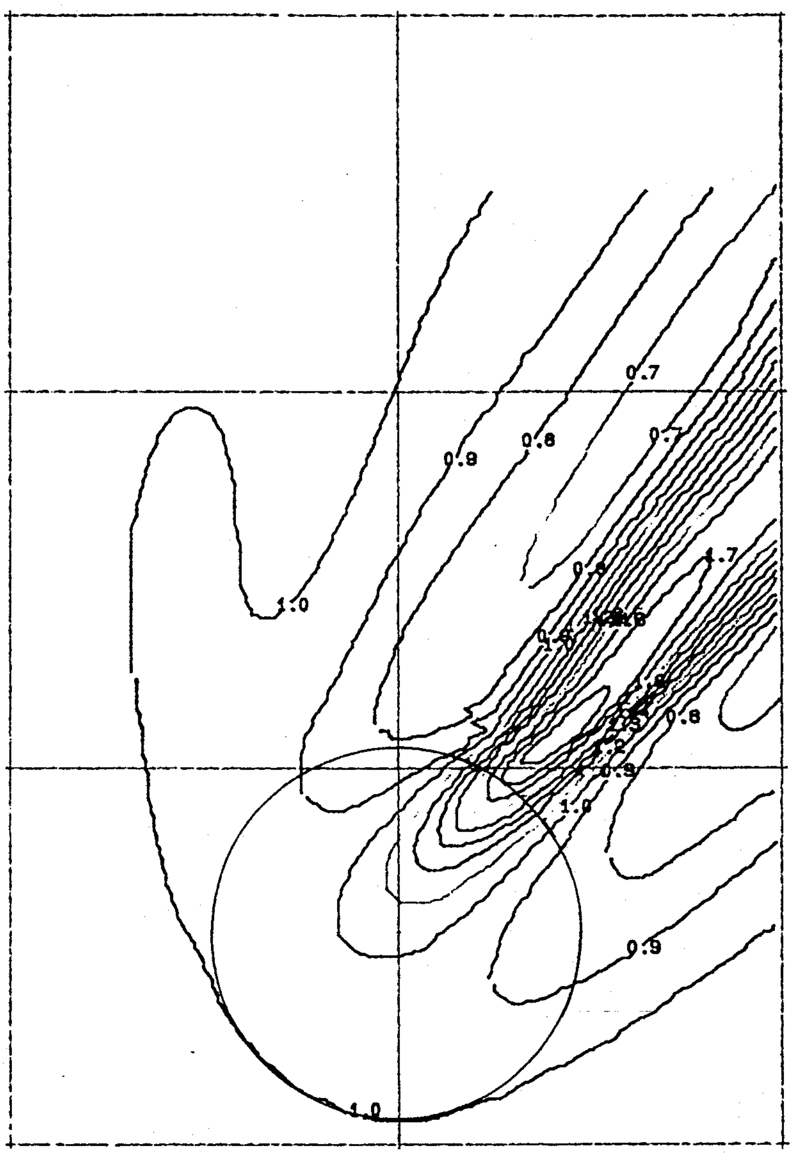

Fig 10 Wave amplitude contours, 50° incident direction, fine grid, averaging number=3

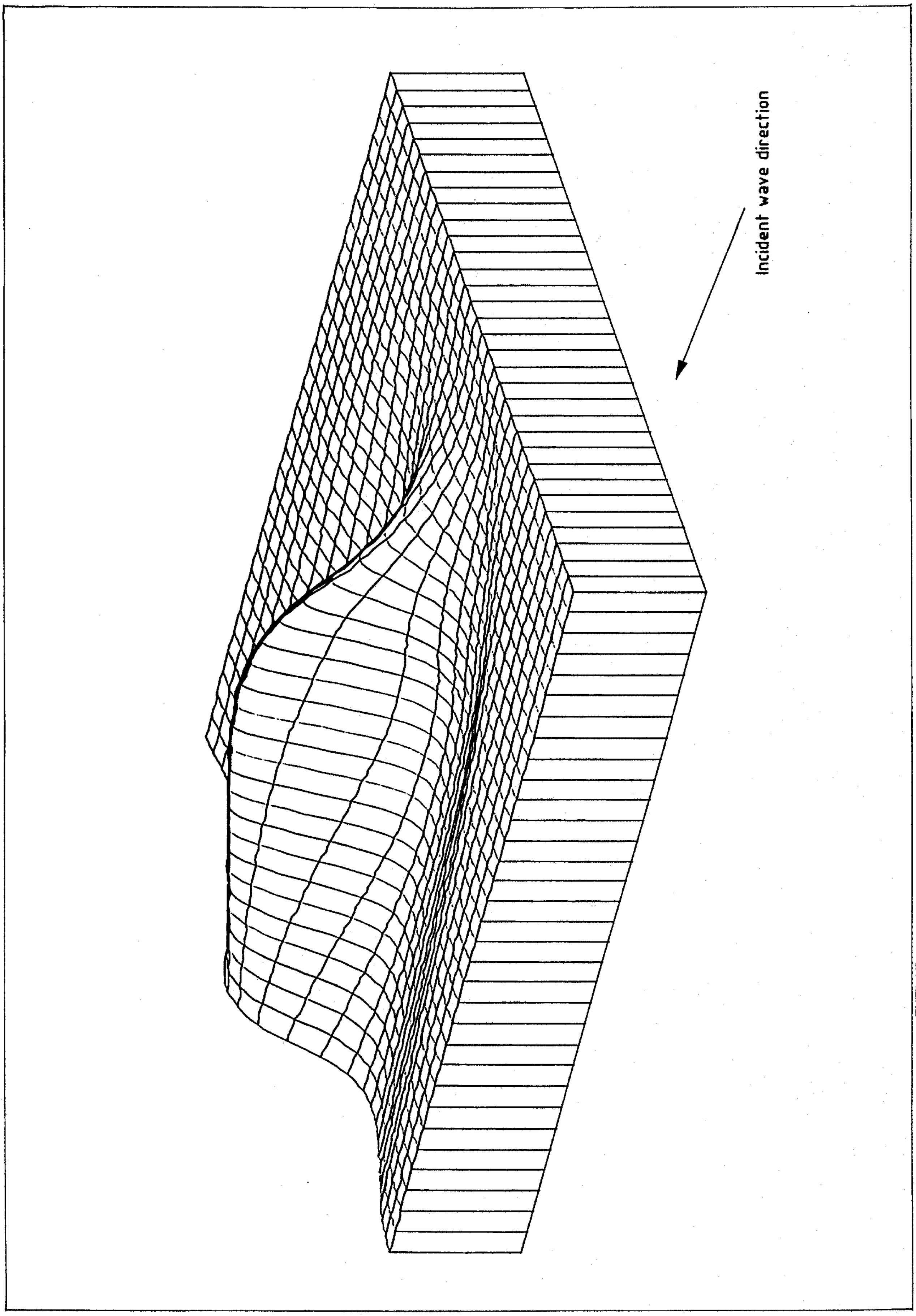

Fig. 11 Isometric plot of wave amplitude, 90° incident direction.

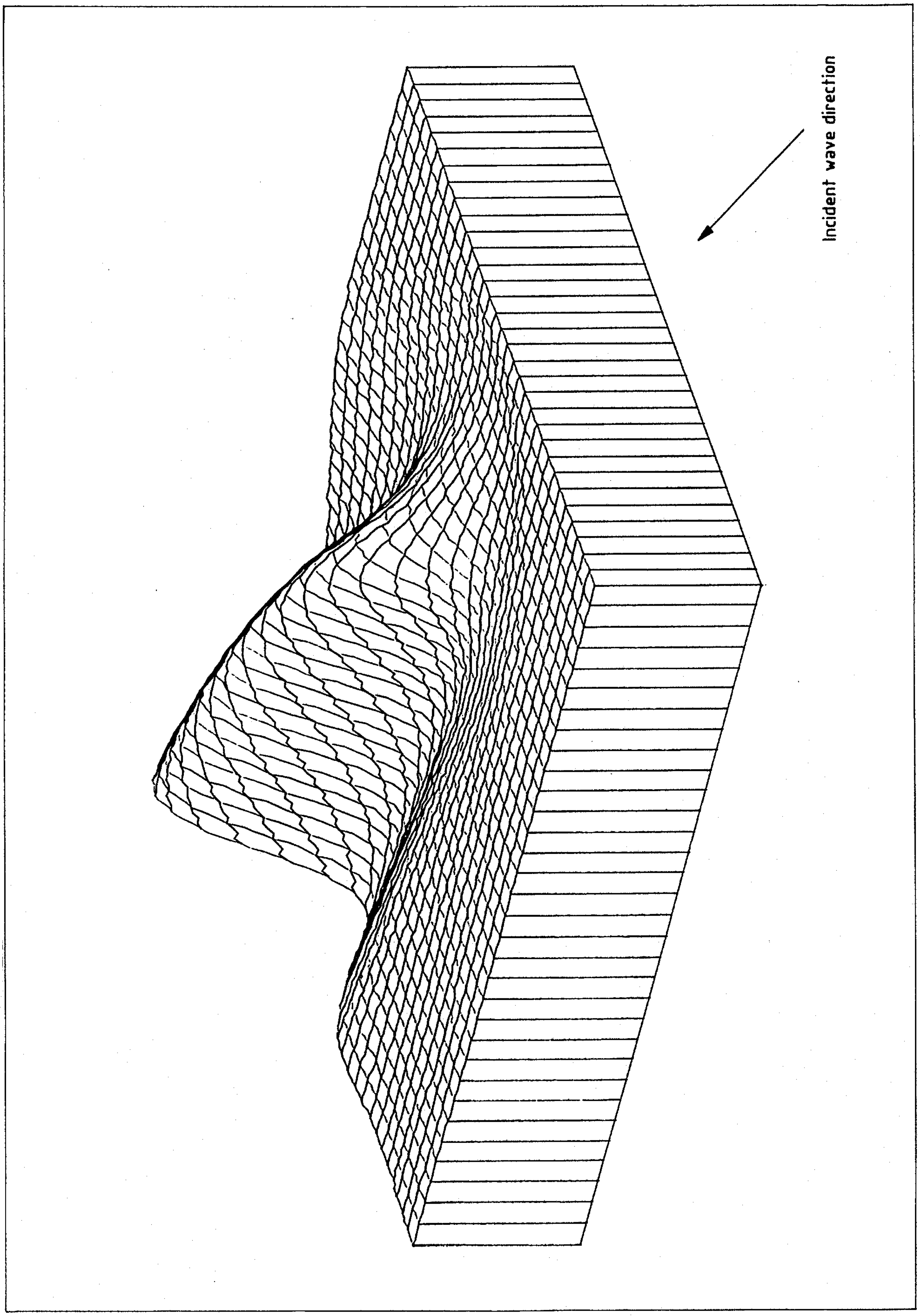

Fig. 12 Isometric plot of wave amplitude,70° incident direction.

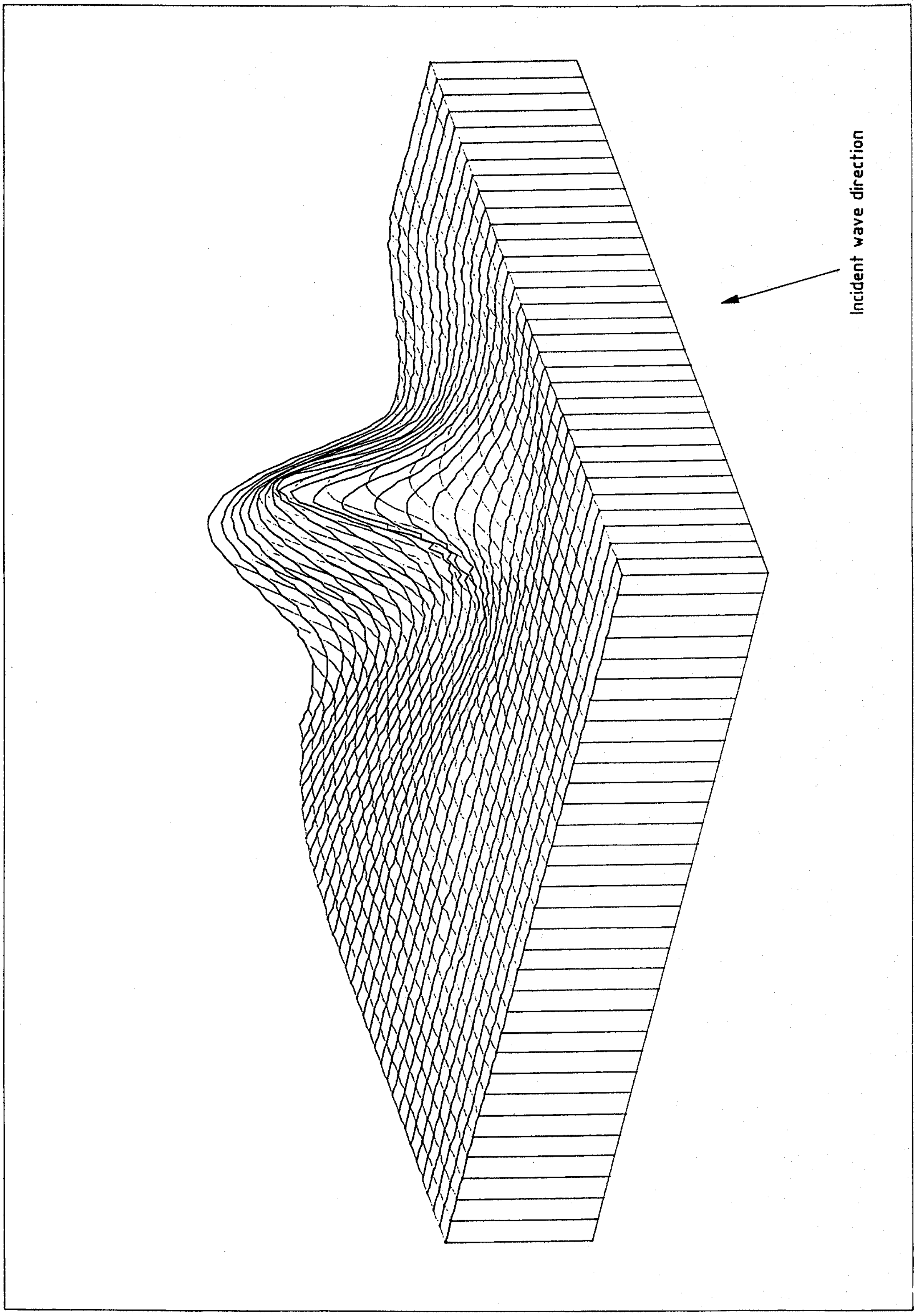

Fig. 13 Isometric plot of wave amplitude,50° incident direction.